Focusing of High-Brightness Electron Beams with Active-Plasma Lenses

R. Pompili,[1,*] M. P. Anania,[1] M. Bellaveglia,[1] A. Biagioni,[1] S. Bini,[1] F. Bisesto,[1] E. Brentegani,[1] F. Cardelli,[1] G. Castorina,[2] E. Chiadroni,[1] A. Cianchi,[3] O. Coiro,[1] G. Costa,[1] M. Croia,[1] D. Di Giovenale,[1] M. Ferrario,[1] F. Filippi,[1] A. Giribono,[1] V. Lollo,[1] A. Marocchino,[1] M. Marongiu,[2] V. Martinelli,[1] A. Mostacci,[2] D. Pellegrini,[1] L. Piersanti,[1] G. Di Pirro,[1] S. Romeo,[1] A. R. Rossi,[4] J. Scifo,[1] V. Shpakov,[1] A. Stella,[1] C. Vaccarezza,[1] F. Villa,[1] and A. Zigler[1,5]

[1]*Laboratori Nazionali di Frascati, Via Enrico Fermi 40, 00044 Frascati, Italy*
[2]*Sapienza University, Piazzale Aldo Moro 5, 00185 Rome, Italy*
[3]*University or Rome Tor Vergata and INFN, Via Ricerca Scientifica 1, 00133 Rome, Italy*
[4]*INFN Milano, via Celoria 16, 20133 Milan, Italy*
[5]*Racah Institute of Physics, Hebrew University, 91904 Jerusalem, Israel*

Plasma-based technology promises a tremendous reduction in size of accelerators used for research, medical, and industrial applications, making it possible to develop tabletop machines accessible for a broader scientific community. By overcoming current limits of conventional accelerators and pushing particles to larger and larger energies, the availability of strong and tunable focusing optics is mandatory also because plasma-accelerated beams usually have large angular divergences. In this regard, active-plasma lenses represent a compact and affordable tool to generate radially symmetric magnetic fields several orders of magnitude larger than conventional quadrupoles and solenoids. However, it has been recently proved that the focusing can be highly nonlinear and induce a dramatic emittance growth. Here, we present experimental results showing how these nonlinearities can be minimized and lensing improved. These achievements represent a major breakthrough toward the miniaturization of next-generation focusing devices.

High-brightness electron beams are nowadays used for many applications such as, for instance, the generation of THz [1,2] and free-electron laser radiation [3,4], inverse Compton scattering [5,6] and transmission electron microscopy [7]. The technology employed to generate such beams is still based on the use of conventional rf accelerators with a limited range of improvement [8,9]. Plasma-based acceleration [10,11] can strongly push toward the development of new compact machines, allowing us to squeeze the accelerating structures down to the centimeter scale [12–15]. In parallel, we have also to foresee new focusing devices with tiny sizes. So far, permanent-magnet quadrupoles represent the state of the art providing focusing gradients of the order of 600 T/m [16,17]. Nevertheless, their focusing is nonsymmetric and the gradient fixed thus nontrivial movable systems (consisting of at least three lenses) must be implemented to produce round beams with (slightly) adjustable focal length.

Radially symmetric focusing with even larger magnetic gradient (of the order of kT/m) has been demonstrated for both electron [18–21] and ion [22–24] beams by means of plasma-based lenses [25–27]. Several results have been also obtained with the so-called "active" plasma lens (APL) [28], showing the focusing of relativistic electron beams both from laser-plasma [29,30] and rf [31–34] accelerators. These devices consist of a discharge current (flowing through a capillary) that generates an azimuthally magnetic field with radially increasing strength [35,36]. However, we have recently proved in two different works [31,32] that such a focusing is highly nonlinear (due to the nonuniformity of the discharge current [37]) and leads to a large growth of the beam emittance. In this Letter, we report about experimental measurements demonstrating that the beam emittance can be preserved (and lensing effect improved) by properly shaping the beam transverse profile and by enhancing the linearity of the focusing field (through an increase of the plasma temperature that, in turn, makes the discharge current more uniform). The experiment has been performed at the SPARC_LAB test facility [38,39] by employing a 3 cm–long discharge capillary filled by hydrogen gas [40]. The characterization of the APL is done by using a 50 pC high-brightness electron beam as a probe and analyzing how the focusing influences its emittance.

The experimental setup is shown in Fig. 1. The bunch is produced by the SPARC photoinjector [41,42], consisting of a 1.6 cell rf gun [43] followed by two accelerating sections embedded in solenoid coils [44,45]. The electron bunch has a 50 pC charge, 127 MeV energy (70 keV energy spread) and 1.3 ps duration, measured with a rf-deflector device [46]. Its normalized emittance on the horizontal (vertical) plane is $\epsilon_{x(y)} \approx 0.8(0.5)$ μm. All these quantities
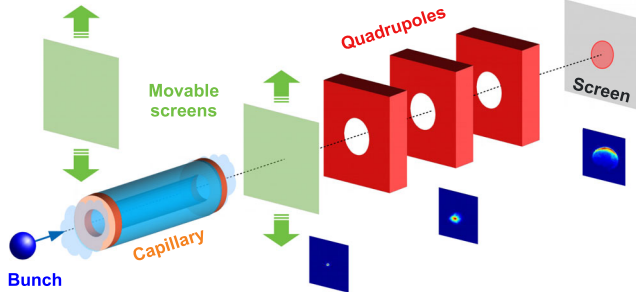
FIG. 1. Experimental layout. Several screens allow us to measure the beam envelope along the path. The first two, located at $z = 0$ (capillary entrance) and $z = 23$ cm, are mounted on movable actuators. Three electromagnetic quadrupoles (at $z = 0.8$ m, $z = 1.1$ m, and $z = 1.3$ m) are used to measure the beam emittance on the last screen, located at $z = 5.2$ m.

are quoted as rms. To test the APL focusing we varied the bunch transverse spot size at the capillary entrance from $\sigma_{x,y} \approx 35$ μm up to $\sigma_{x,y} \approx 160$ μm. This is the largest spot size that ensures to transport the entire beam charge (measured with a beam current monitor) across the capillary clear aperture. These measurements have been done by using a transition radiation (TR) screen installed at the capillary entrance. The beam envelope evolution along the entire path is finally measured by using several Ce:YAG screens installed along the photoinjector. The last one, about 5.2 m downstream of the capillary, is also used for emittance measurements through quadrupole scan [47,48] using a triplet of electromagnetic quadrupoles installed upstream.

The APL consists of a sapphire tube with length $L_c = 3$ cm and $R_c = 500$ μm hole radius. The capillary is filled at 1 Hz rate with H_2 gas (produced by an electrolytic generator) through two inlets placed at $L_c/4$ and $3L_c/4$ and has two electrodes at its extremities connected to the discharge circuit fed by a 20 kV pulser [49]. The timing jitter

between the pulser and the electron beam is approximately 10 ns. The peak plasma density reached in the capillary is $n_p \approx 2 \times 10^{17}$ cm^{-3}, estimated by measuring the H_β Balmer line with a Stark broadening-based diagnostics [40]. The capillary is installed in a vacuum chamber directly connected with a windowless, three-stage differential pumping system that ensures 10^{-8} mbar pressure in the rf linac while flowing H_2. This solution allows us to transport the beam without encountering any window, thus not degrading its emittance by multiple scattering. Based on the findings of our previous works we moved to a new discharge circuit able to provide currents larger than $I_D \approx 100$ A and up to $I_D \approx 230$ A. The resulting waveform is reported in Fig. 2(a). Such a current ensures that almost 90% of H_2 is ionized [50] (previously it was barely 30%) and larger temperatures reached (up to 4 eV). We show in Fig. 2(b) the expected radial profiles of the magnetic field and plasma temperature calculated with a one-dimensional analytical model [51]. The model computes the radial profile of plasma temperature $T(r)$ across the capillary, allowing retrieving the profile of the current density as $J(r) = \sigma_e(r)E$, with $\sigma_e \propto T(r)^{3/2}$ the electric conductivity and E the electric field associated with the discharge current [52]. The enhanced linearity of the magnetic field, computed from the Ampère law $B_\varphi(r) = \mu_0 r^{-1} \int_0^r J(r')r'dr'$, is due to the increased plasma conductivity associated to the larger discharge current [35].

In the following, we discuss the plasma lens dynamics by comparing its response to different spot sizes (i.e., bunch densities). It is well known that the interaction with plasma generates beam-driven wakefields that can strongly affect the bunch dynamics [20]. In this context, passive plasma lenses have been widely investigated [18,19] and are able produce a net beam focusing through the plasma neutralization of the space-charge fields. In our specific case we refer to the so-called *overdense* passive lenses where $n_b \ll n_p$, with n_b
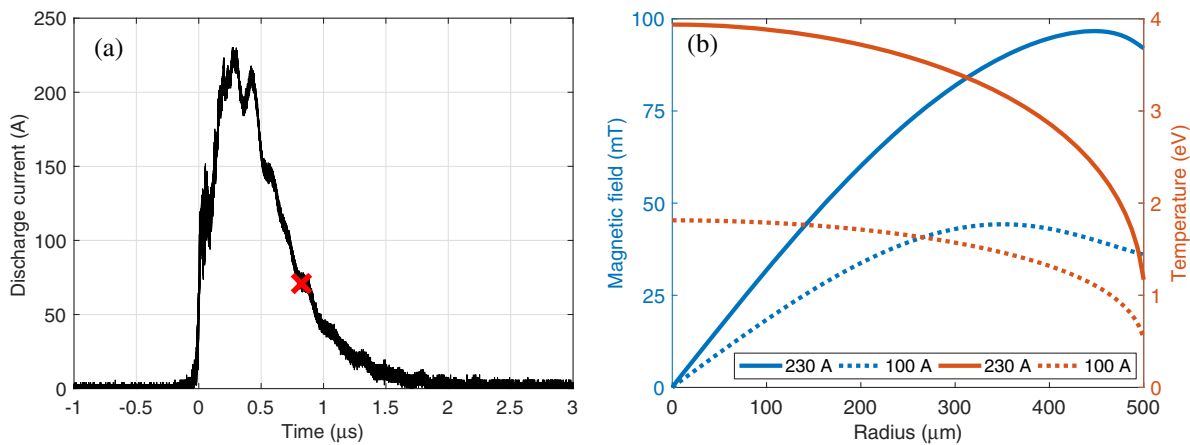

FIG. 2. (a) Discharge current waveform obtained by averaging 20 consecutive shots. The red cross indicates the effective current that produces the smallest spot size on the first screen downstream of the capillary. (b) Calculated radial profiles of the azimuthal magnetic field (blue) and temperature (red) across the capillary. The solid (dotted) lines are obtained when plasma is produced by a 230 A (100 A) discharge current.

indicating the bunch density. When dealing with active-plasma lenses we have therefore to consider their combined effect [32]. The nonlinearities of the overall focusing can be minimized by manipulating both the bunch shape and the capillary-discharge setup. The strength of the radial plasma wakefield is governed both by n_b and n_p [53] and its effect can be reduced by decreasing both, i.e., by operating with low plasma densities or by entering into the plasma with a large transverse spot (corresponding to a lower n_b [30]). On the contrary, the linearity of the APL field is guaranteed only at small radii since the magnetic field toward the capillary walls bends down, as shown in Fig. 2(b). It implies that small transverse spots are in this case preferable.

Figure 3 shows the bunch emittance measured downstream of the capillary as a function of the spot size at its entrance. Each point is obtained for the minimum spot provided by the APL on the first screen. The tuning is achieved by delaying the discharge-current trigger with respect to the beam arrival time. For our experimental setup it corresponded to an effective current of $I_D \approx 70$ A, as indicated in Fig. 2(a). In the plot we have included the measured horizontal and vertical emittances and the expectations from numerical simulation (more details given later). We clearly see that for small spot sizes ($\sigma_{x,y} \approx 30$ μm), there is a strong effect of the plasma wakefields due to the larger bunch density ($n_b \approx 10^{14}$ cm^{-3}). In this case the bunch emittance increases up to $\epsilon_{x,y} \approx 9$ μm. Conversely, for large spot sizes ($\sigma_{x,y} \approx 160$ μm, corresponding to $n_b \approx 3 \times 10^{12}$ cm^{-3}) their effect is minimized but the nonlinearities of the active lensing also increase the emittance (up to $\epsilon_{x,y} \approx 3$ μm).

According to simulations of Fig. 3, the best compromise in terms of resulting emittance is obtained by entering into

the plasma with a transverse spot size $\sigma_{x,y} \approx 110$ μm. We thus followed this expectation and tuned the magnetic optics along the photoinjector to achieve an experimental spot size at capillary entrance of $\sigma_{x,y} = 115 \pm 5$ μm. Figure 4(a) shows the unperturbed beam ($\sigma_{x,y} = 105 \pm 4$ μm) as obtained when the discharge is turned off. Here the beam is detected on the first Ce:YAG screen downstream of the capillary (≈ 20 cm far from it). When the discharge is turned on and its delay adjusted to provide the minimum spot size on such a screen ($I_D \approx 70$ A), the beam is squeezed to $\sigma_{x,y} = 17.5 \pm 0.3$ μm as shown in Fig. 4(b) (it was 24 ± 3 μm with the old 100 A discharge circuit [31]). These conditions correspond also to the best results in terms of beam emittance, equal to $\epsilon_{x,y} \approx 0.9$ μm. With respect to the unperturbed beam, these numbers say that such a quantity is almost preserved, at least considering the horizontal plane. The complete envelope scan obtained with different focusing strengths is reported in Fig. 4(c). Each color refers to a different relative delay between the electron bunch and discharge current. The solid lines represent the computed numerical simulation of the bunch envelope evolution while the data points are experimental measurements on the first screen downstream of the APL. The strongest focusing (and, thus, the shortest focal length) is obtained when the bunch is
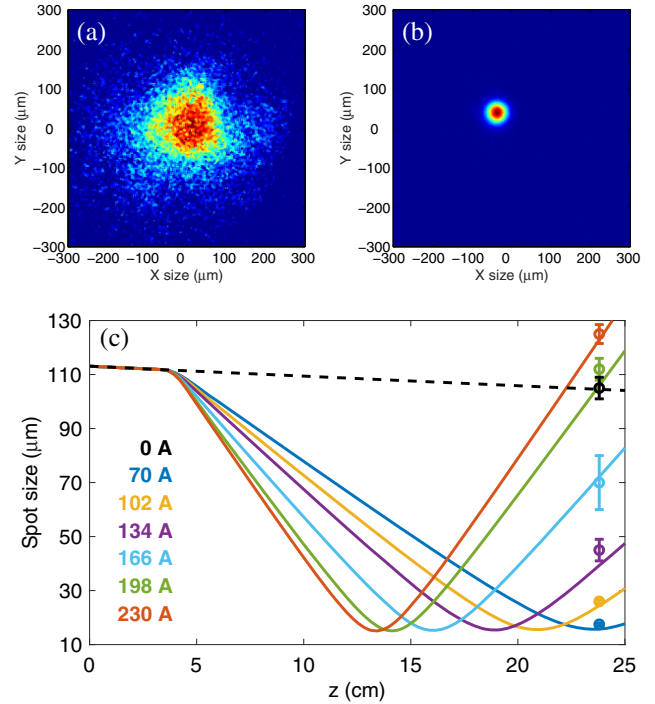
FIG. 4. Bunch spot measured on the first screen downstream of the capillary with the discharge turned off [(a) $\sigma_{x,y} = 105 \pm 4$ μm] and on [(b) $\sigma_{x,y} = 17.5 \pm 0.3$ μm]. (c) Experimental spot sizes (circles) obtained on the same screen for different discharge currents. The envelopes computed by simulations (solid lines) are also reported. The dashed line refers to the beam envelope obtained with the discharge turned off.
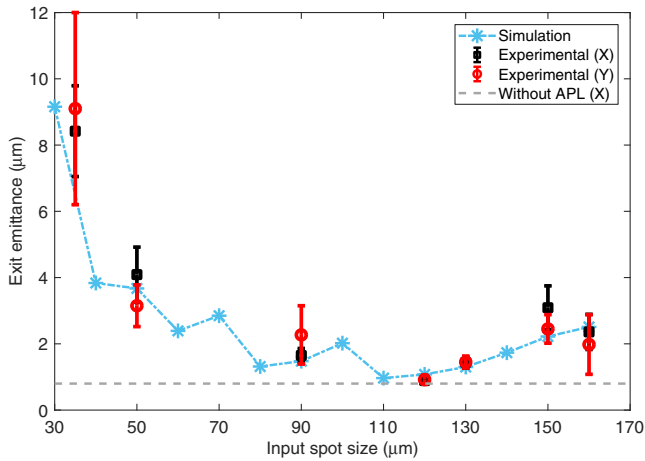

FIG. 3. Resulting emittance as a function of the beam spot size at capillary entrance. The black (red) data points refer to the experimentally measured $X(Y)$ emittances. The blue line reports the expected emittance obtained with numerical simulations. The gray line shows the unperturbed (X) beam emittance without APL.

focused at the discharge-current peak ($\approx$230 A). Here the expected waist is about 14 μm.

The beam exiting from the APL travels approximately 1 m before entering into the emittance measurement quadrupoles and about 5.2 m before reaching the screen where it is detected. By considering also its large divergence ($\approx$1 mrad), we have to take into account that the quadrupole-scan technique could be affected by chromatic effects associated to so large spot sizes at the quadrupole entrance and eventually results in a wrong estimation of the beam emittance [47]. To validate the measurements we have computed a start-to-end simulation for the beam exiting the APL by using the general particle tracer (GPT) code [54] and reproducing all the focusing optics of the SPARC_LAB photoinjector. Figure 5 shows the resulting quadrupole scan with both the experimental points (blue circles) and the simulated ones (green line). The emittance value is obtained by fitting the experimental data (red line). We found that by applying the same fitting algorithm on the simulated data, the discrepancy is

about 3%. For the sake of completeness we have also compared these results with the analytic expressions provided in Ref. [47], resulting in a deviation of 2%. We conclude therefore that even with so large spot sizes, the energy spread is low enough and chromatic effects can be neglected.

The study on such a beam configuration is completed by analyzing its evolution through the plasma channel with the discharge current turned on. Considering that we are working in the overdense regime, the interaction can be described with classical 2D plasma wakefield theory in linear regime [55,56]. The simulation also takes into account the finite plasma radial extension, being confined within the capillary radius R_c [57]. Following our previous studies in which we completely characterized the longitudinal plasma density profile along the capillary, here the channel is numerically computed by assuming a flat profile in the central part with decreasing exponential tails extending 1 cm outside the capillary [40,58,59]. Figure 6(a) shows
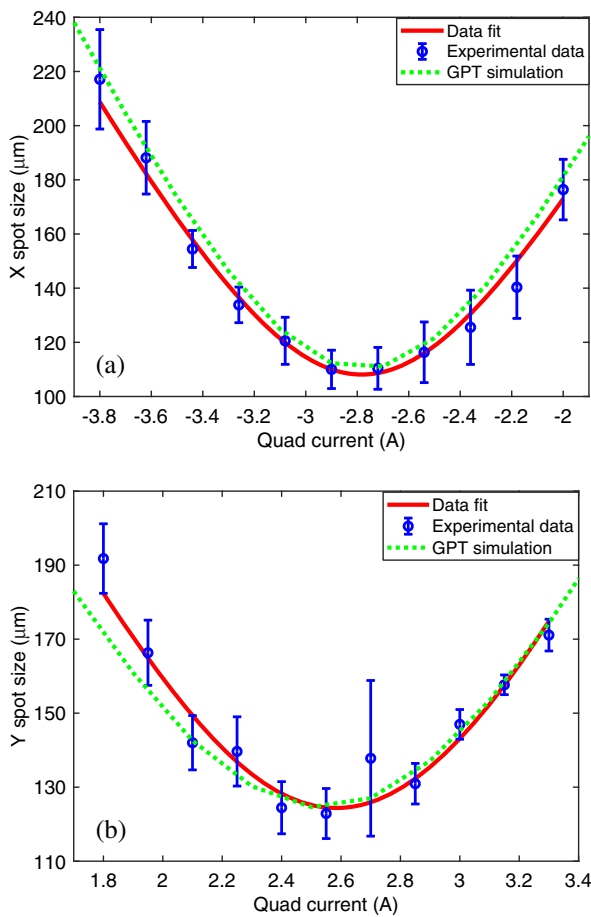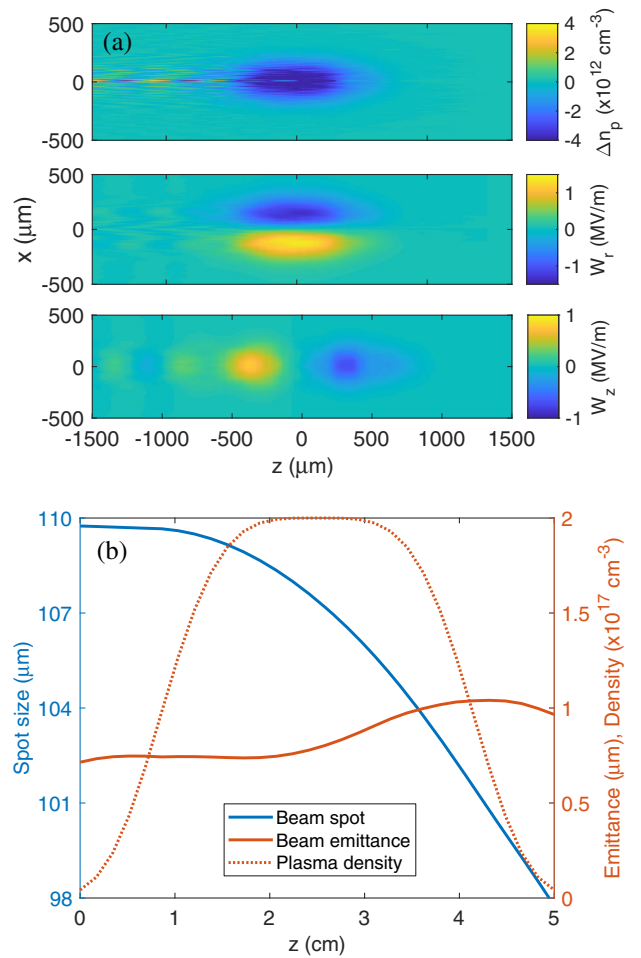

FIG. 5. Measurement of the normalized emittance with quadrupole-scan technique of the bunch exiting from the APL. The horizontal axis reports the quadrupole currents while the vertical one shows the horizontal (a) and vertical (b) spot sizes. The red line shows the computed fit used to evaluate the emittance value. The dotted green line reproduces the quadrupole scan obtained with GPT simulation.

FIG. 6. (a) Simulation of the perturbed plasma density (top) profile at the entrance of the plasma and computed radial (W_r, center) and longitudinal (W_z, bottom) wakefields. (b) Bunch envelope (blue) and normalized emittance (red) evolution along the plasma. The red dashed line shows the simulated plasma density profile (3 cm–long capillary with 1 cm input and exit ramps).

a snapshot of the perturbed plasma density (Δn_p) and of the radial (W_r) and longitudinal (W_z) wakefields induced by the traveling bunch. The evolution of the beam envelope and emittance is shown in Fig. 6(b). The dotted line represents the simulated longitudinal plasma density profile. As expected there is a weak passive lens focusing in the first plasma ramp ($I_D = 0$) that also induces a slight emittance increase. Within the capillary ($I_D \neq 0$), the external discharge current increases the beam focusing and triggers an emittance oscillation that is completed in the last plasma ramp ($I_D = 0$). At the end of the path the beam emittance is $\epsilon_{x,y} \approx 0.9 \ \mu$m, in agreement with the measured one.

In conclusion, we have presented a complete characterization of an active-plasma lens device consisting of a 3 cm–long capillary filled by H_2 gas. Starting from our previous works, we modified the arrangement of our experimental setup to optimize the provided lensing and preserve the beam emittance. Here, we have demonstrated that by increasing the discharge current flowing through the capillary and with a proper bunch shaping, the detrimental effects induced on the beam dynamics are minimized. Once tuned, the system allowed us to reach a stronger focusing that resulted in a beam waist of 17 μm and minimal increase of the horizontal beam emittance ($\approx$12%), although the growth is more pronounced on the vertical plane ($\approx$80%). Such an asymmetry might be due to some inhomogeneities on the vertical profile of the discharge current induced by the presence of the two inlets (in the upper side of the capillary) and is currently under investigation. It is worth pointing out that the preservation of the beam emittance is a key requirement when dealing with high-brightness beams. These results represent thus a fundamental step toward the development of next-generation focusing optics and demonstrate their effective usability in view of new compact facilities.

---

[*]riccardo.pompili@lnf.infn.it

[1] E. Chiadroni, M. Bellaveglia, P. Calvani, M. Castellano, L. Catani, A. Cianchi, G. D. Pirro, M. Ferrario, G. Gatti, O. Limaj, S. Lupi, B. Marchetti, A. Mostacci, E. Pace, L. Palumbo, C. Ronsivalle, R. Pompili, and C. Vaccarezza, Rev. Sci. Instrum. **84**, 022703 (2013).

[2] F. Giorgianni *et al.*, Nat. Commun. **7**, 11421 (2016).

[3] W. Ackermann *et al.*, Nat. Photonics **1**, 336 (2007).

[4] V. Petrillo, Phys. Rev. Lett. **111**, 114802 (2013).

[5] R. W. Schoenlein, W. Leemans, A. Chin, and P. Volfbeyn, Science **274**, 236 (1996).

[6] A. Bacci *et al.*, J. Appl. Phys. **113**, 194508 (2013).

[7] R. K. Li and P. Musumeci, Phys. Rev. Applied **2**, 024003 (2014).

[8] M. Dal Forno, V. Dolgashev, G. Bowden, C. Clarke, M. Hogan, D. McCormick, A. Novokhatski, B. O'Shea, B. Spataro, S. Weathersby, and S. G. Tantawi, Phys. Rev. Accel. Beams **19**, 111301 (2016).

[9] E. I. Simakov, V. A. Dolgashev, and S. G. Tantawi, Nucl. Instrum. Methods Phys. Res., Sect. A **907**, 221 (2018).

[10] T. Tajima and J. M. Dawson, Phys. Rev. Lett. **43**, 267 (1979).

[11] P. Chen, J. M. Dawson, R. W. Huff, and T. Katsouleas, Phys. Rev. Lett. **54**, 693 (1985).

[12] I. Blumenfeld, C. E. Clayton, F.-J. Decker, M. J. Hogan, C. Huang, R. Ischebeck, R. Iverson, C. Joshi, T. Katsouleas, N. Kirby, W. Lu, K. A. Marsh, W. B. Mori, P. Muggli, E. Oz, R. H. Siemann, D. Walz, and M. Zhou, Nature (London) **445**, 741 (2007).

[13] W. Leemans, B. Nagler, A. Gonsalves, C. Tóth, K. Nakamura, C. Geddes, E. Esarey, C. Schroeder, and S. Hooker, Nat. Phys. **2**, 696 (2006).

[14] M. Litos *et al.*, Nature (London) **515**, 92 (2014).

[15] S. Steinke *et al.*, Nature (London) **530**, 190 (2016).

[16] J. Lim, P. Frigola, G. Travish, J. Rosenzweig, S. Anderson, W. Brown, J. Jacob, C. Robbins, and A. Tremaine, Phys. Rev. ST Accel. Beams **8**, 072401 (2005).

[17] R. Pompili *et al.*, Rev. Sci. Instrum. **89**, 033302 (2018).

[18] J. J. Su, T. Katsouleas, J. M. Dawson, and R. Fedele, Phys. Rev. A **41**, 3321 (1990).

[19] G. Hairapetian, P. Davis, C. E. Clayton, C. Joshi, S. C. Hartman, C. Pellegrini, and T. Katsouleas, Phys. Rev. Lett. **72**, 2403 (1994).

[20] R. Govil, W. P. Leemans, E. Y. Backhaus, and J. S. Wurtele, Phys. Rev. Lett. **83**, 3202 (1999).

[21] C. Thaury *et al.*, Nat. Commun. **6**, 6860 (2015).

[22] E. Boggasch, J. Jacoby, H. Wahl, K.-G. Dietrich, D. H. H. Hoffmann, W. Laux, M. Elfers, C. R. Haas, V. P. Dubenkov, and A. A. Golubev, Phys. Rev. Lett. **66**, 1705 (1991).

[23] E. Boggasch, A. Tauschwitz, H. Wahl, K.-G. Dietrich, D. Hoffmann, W. Laux, M. Stetter, and R. Tkotz, Appl. Phys. Lett. **60**, 2475 (1992).

[24] A. Tauschwitz, S. Yu, S. Eylon, R. Bangerter, W. Leemans, C. Peters, J. Rasmussen, L. Reginato, J. Barnard, and W. Sharp, Fusion Eng. Des. **32-33**, 493 (1996).

[25] P. Chen, K. Oide, A. M. Sessler, and S. S. Yu, Phys. Rev. Lett. **64**, 1231 (1990).

[26] J. B. Rosenzweig, B. Breizman, T. Katsouleas, and J. J. Su, Phys. Rev. A **44**, R6189 (1991).

[27] H. Nakanishi *et al.*, Phys. Rev. Lett. **66**, 1870 (1991).

[28] W. K. H. Panofsky and W. Baker, Rev. Sci. Instrum. **21**, 445 (1950).

[29] J. van Tilborg, Phys. Rev. Lett. **115**, 184802 (2015).

[30] J. van Tilborg, S. Barber, C. Benedetti, C. Schroeder, F. Isono, H.-E. Tsai, C. Geddes, and W. Leemans, Phys. Plasmas **25**, 056702 (2018).

[31] R. Pompili *et al.*, Appl. Phys. Lett. **110**, 104101 (2017).

[32] A. Marocchino *et al.*, Appl. Phys. Lett. **111,** 184101 (2017).

[33] E. Chiadroni *et al.*, Nucl. Instrum. Methods Phys. Res., Sect. A, doi: 10.1016/j.nima.2018.02.014 (2018).

[34] C. Lindstrøm *et al.*, Nucl. Instrum. Methods Phys. Res., Sect. A, doi: 10.1016/j.nima.2018.01.063 (2018).

[35] G. Bagdasarov *et al.*, Phys. Plasmas **24,** 053111 (2017).

[36] R. Pompili, G. Castorina, M. Ferrario, A. Marocchino, and A. Zigler, AIP Adv. **8,** 015326 (2018).

[37] J. van Tilborg *et al.*, Phys. Rev. Accel. Beams **20,** 032803 (2017).

[38] M. Ferrario *et al.*, Nucl. Instrum. Methods Phys. Res., Sect. B **309,** 183 (2013).

[39] R. Pompili *et al.*, Nucl. Instrum. Methods Phys. Res., Sect. A, doi: 10.1016/j.nima.2018.01.071 (2018).

[40] F. Filippi, M. Anania, A. Biagioni, E. Chiadroni, A. Cianchi, M. Ferrario, A. Mostacci, L. Palumbo, and A. Zigler, J. Instrum. **11,** C09015 (2016).

[41] D. Alesini *et al.*, Nucl. Instrum. Methods Phys. Res., Sect. A **507,** 345 (2003).

[42] E. Chiadroni *et al.*, Appl. Phys. Lett. **102,** 094101 (2013).

[43] A. Cianchi *et al.*, Phys. Rev. ST Accel. Beams **11,** 032801 (2008).

[44] M. Ferrario *et al.*, Phys. Rev. Lett. **104,** 054801 (2010).

[45] R. Pompili *et al.*, Nucl. Instrum. Methods Phys. Res., Sect. A **829,** 17 (2016).

[46] D. Alesini, G. Di Pirro, L. Ficcadenti, A. Mostacci, L. Palumbo, J. Rosenzweig, and C. Vaccarezza, Nucl. Instrum. Methods Phys. Res., Sect. A **568,** 488 (2006).

[47] A. Mostacci, M. Bellaveglia, E. Chiadroni, A. Cianchi, M. Ferrario, D. Filippetto, G. Gatti, and C. Ronsivalle, Phys. Rev. ST Accel. Beams **15,** 082802 (2012).

[48] A. Cianchi *et al.*, Phys. Rev. ST Accel. Beams **18,** 082804 (2015).

[49] M. Anania *et al.*, Nucl. Instrum. Methods Phys. Res., Sect. A **829,** 254 (2016).

[50] E. Brentegani *et al.*, Nucl. Instrum. Methods Phys. Res., Sect. A, doi: 10.1016/j.nima.2018.03.012 (2018).

[51] N. A. Bobrova, A. A. Esaulov, J.-I. Sakai, P. V. Sasorov, D. J. Spence, A. Butler, S. M. Hooker, and S. V. Bulanov, Phys. Rev. E **65,** 016407 (2001).

[52] S. Eliezer, *The Interaction of High-Power Lasers with Plasmas* (CRC Press, Boca Raton, FL, 2002).

[53] P. Chen, J. Su, T. Katsouleas, S. Wilks, and J. Dawson, IEEE Trans. Plasma Sci. **15,** 218 (1987).

[54] S. B. Van Der Geer, O. J. Luiten, M. J. De Loos, G. Pöplau, and U. Van Rienen, *3D Space-Charge Model for GPT Simulations of High Brightness Electron Bunches*, Institute of Physics Conference Series Vol. 175 (2005), p. 101.

[55] W. Lu, C. Huang, M. Zhou, W. Mori, and T. Katsouleas, Phys. Plasmas **12,** 063101 (2005).

[56] A. Marocchino, F. Massimo, A. Rossi, E. Chiadroni, and M. Ferrario, Nucl. Instrum. Methods Phys. Res., Sect. A **829,** 386 (2016).

[57] Y. Fang, J. Vieira, L. Amorim, W. Mori, and P. Muggli, Phys. Plasmas **21,** 056703 (2014).

[58] A. Biagioni *et al.*, J. Instrum. **11,** C08003 (2016).

[59] F. Filippi *et al.*, Nucl. Instrum. Methods Phys. Res., Sect. A, doi: 10.1016/j.nima.2018.04.037 (2018).